Copyright © 2013 Tech Science Press CMES, vol.91, no.2, pp.81-100, 2013

Numerical study on seepage property of karst collapse columns under particle migration

Banghua Yao[1,2], Jianping Wei[1], Dengke Wang[1], Dan Ma[2,3], Zhanqing Chen[2]

Abstract: Presently, there is an increasing number of water outburst accidents in China as mining activity continues to develop to deeper ground. In these accidents, water outburst caused by karst collapse columns often results in serious damage, involving both the loss of lives and significant economic loss. Therefore, it is of utmost importance to study the seepage property and water outburst mechanism of karst collapse columns. In this paper, based on the seepage theory and the groundwater dynamic theory of porous media, a fluid-solid coupling model for karst collapse columns was built and then imported into COMSOL Multiphysics to be solved, by considering the heterogeneity of rocks in karst collapse columns, and assuming that the porosity obey Weibull distribution, thus obtained the parameters, including porosity, seepage, particle concentration, water inflow evolution law. The research results indicate the following: (1) particles in karst collapse columns will be eroded and transported under the effect of fluid as the time, porosity, water inflow and particle migration velocity all increase rapidly, and eventually a main seepage channel will form; (2) the seepage capacity for karst collapse columns initially grows slowly, then water inflow increases gradually with the erosion and migration of the particles.

Keywords: karst collapse column; seepage property; particle migration; numerical simulation

1 Introduction

As mining activity rapidly develops to deeper and deeper ground, there has been an increasing number of water outburst accidents occurring in China. In these ac-

[1] State Key Laboratory Cultivation Base for Gas Geology and Gas control (Henan Polytechnic University), Jiaozuo, Henan 454000, China

[2] State Key Laboratory for Geomechanics & Deep Underground Engineering, China University of Mining & Technology, Xuzhou 221008, China

[3] Corresponding author, madancumt@gmail.com

cidents, water outbursts caused by karst collapse columns (Figure 1) often result in serious disaster, involving both the loss of lives and significant economic loss. For example, on June, 2, 1984, a karst collapse column water outburst accident with a world record water inflow volume of 2053 m^3/min occurred at Fangezhuang coal mine in Hebei Province, China, which resulted in the direct economic loss of 500 million RMB; and in 2010, Luotuo coal mine in Inner Mongolia experienced a karst collapse column water outburst, causing direct economic loss of 48.53 million RMB and the death of 32 people. Therefore, water-conducted karst collapse columns have become hidden problems which threaten and influence the safety of mining in many mining areas of China.

In order to explore the water outburst mechanism of water-conducted karst collapse columns, many researchers in China have performed much useful work. For instance, in our previous work, we established a mechanical model for predicting concealed karst collapse column water outburst (Tang JH, Yao BH et al., 2011); other Chinese researchers have studied the water outburst process of karst collapse columns by using numerical simulation software, and discussed their water outburst mechanism (Zhu WC et al., 2009; Yang TH et al., 2008). In recent years, some researchers have begun to study their water outburst mechanism using experimental methods (Wang JC et al., 2010). However, these investigations were mainly carried out with respect to structure failure, and only a small number of researchers in China have investigated this problem from the perspectives of fluid-solid coupling and particle migration.

In this paper, we consider the water outburst accidents caused by karst collapse columns as the reason of erosion, due to the fact that karst collapse columns may result in porosity and permeability change, thus causing water outburst accidents. Due to the current lack of research in this field in China, we refer to several papers regarding sand erosion and particle migration. For example, the problems of aqueous solutions which flow through a porous rock and react with its mineral components are studied. We also introduce an equation for porosity change rate, and establish an equation for porosity change, fluid advection and diffusion effects (Ortoleve et al., 1987); I. Vardoulakis et al. examined the hydro-mechanical aspect of sand production, set the basic frame of the corresponding mathematical model, and studied the piping and surface erosion effects, based on mass balance, particle migration and as Darcy's law (Vardoulakis et al., 1996). MA Habib investigated the erosion rate correlations of a pipe protruding from an abrupt pipe contraction problem, and presented a numerical investigation of the erosion of a pipe protruding due to a sudden contraction (Habib et al., 2007). Other papers (Papamichos and Vardoulakis, 2005; Yasuhara and Elsworth, 2006; Wang and Wan, 2004; Bouchelaghem and Jozja, 2009; Benmebarek et al., 2005) also provided use-

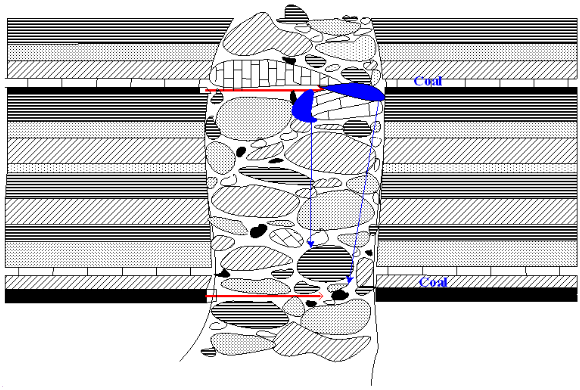

Figure 1: Karst collapse columns in rock strata

ful references for our investigation. Based on the perspective of the fluid-solid coupling effect, our research has significant meaning for revealing the mechanism of water outburst and preventing future water outburst accidents involving karst collapse columns from occurring.

2 Model establishment

2.1 Basic assumption

1. Karst collapse columns may be considered as porous media;
2. Karst collapse columns may be regarded as axisymmetric structures;
3. Migration of fluid and particles in karst collapse columns obey Darcy's law;
4. Concentration of fluidized solid particles in fluid is relatively small, thus impact effects among particles may be neglected.

2.2 2.2 Definition

Based on the above assumptions, we can take a representative element volume (REV), as shown in Figure 2, which consists of the following three constituents: solid(s), fluid(s) and fluidized solid particles, with volumes V_s,V_f,V_{fs} and masses M_s,M_f,M_{fs}, respectively.

Therefore, the void volume in the REV is $V_v = V_f + V_{fs}$, and the porosity of the REV may be expressed as follows:

$$\varphi = \frac{V_v}{V} = \frac{V_f + V_{fs}}{V} \tag{1}$$

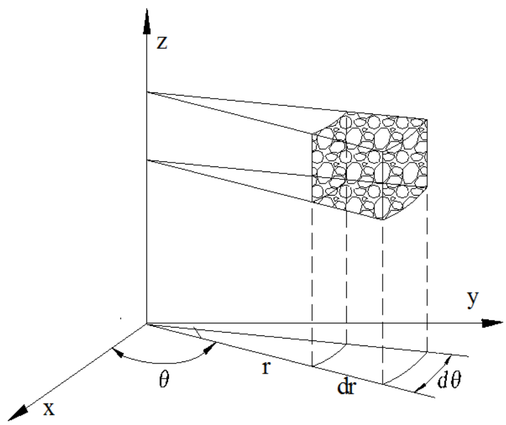

Figure 2: Representative element volume for karst collapse column

The concentration of fluidized solid particles in porosity is expressed as follows:

$$C=\frac{V_{fs}}{V_v}=\frac{V_{fs}}{V_f+V_{fs}},\rho_{fs}=\frac{M_{fs}}{V_v}=C\rho_s \tag{2}$$

2.2.1 Mass balance equations

We assume the coordinate of the REV is $P(r,\theta,z)$, with volume $V=drd\theta dz$.The migration of fluidized solid particles is caused by the coaction of advection and diffusion. For the advection effect along the $z$direction, the lower surface area is $rdrd\theta$, with a velocity of q_{pz}, therefore the fluidized solid particles accumulated in the REV in the z direction during the unit time may be expressed as follows:

$$\frac{\partial(\rho_{fs}q_{pz})}{\partial z}rdrd\theta dz-\frac{\partial}{\partial z}(\varphi D\frac{\partial\rho_{fs}}{\partial z})rdrd\theta dz \tag{3}$$

In addition, the fluidized solid particles accumulated in the REV in the $r$direction during the unit time under the effect of diffusion may be expressed as follows:

$$\frac{\partial(\rho_{fs}q_{pr})}{\partial r}rdrd\theta dz+\rho_{fs}v_{pr}drd\theta dz-\frac{\partial}{\partial r}(\varphi D\frac{\partial\rho_{fs}}{\partial r})rdrd\theta dz-\varphi D\frac{\partial\rho_{fs}}{\partial r}drd\theta dz \tag{4}$$

The model is axisymmetric and the mass accumulation in θ is 0, thus for the REV, the total mass accumulation of fluidized solid particles in the REV is as shown below:

$$\left(\frac{\partial(\rho_{fs}q_{pr})}{\partial r}+\frac{\rho_{fs}q_{pr}}{r}+\frac{\partial(\rho_{fs}q_{pz})}{\partial z}-\frac{\partial}{\partial z}(\phi D\frac{\partial\rho_{fs}}{\partial z})\right.$$
$$\left.-\frac{\partial}{\partial r}(\phi D\frac{\partial\rho_{fs}}{\partial r})-\frac{\phi D}{r}\frac{\partial\rho_{fs}}{\partial r}\right)rdrd\theta dz \quad (5)$$

According to the law of mass conservation, the mass accumulation is equal to the decrease in mass in the REV:

$$-\frac{\partial}{\partial t}(\varphi\rho_{fs}rdrd\theta dz)+\dot{m}rdrd\theta dz \quad (6)$$

where $\dot{m}$ is a mass-generation term, which corresponds to the rate of net mass eroded in the REV during the unit time; then we may obtain the following expression:

$$-\frac{\partial}{\partial t}(\varphi\rho_{fs}rdrd\theta dz)+\dot{m}rdrd\theta dz=$$
$$\left(\frac{\partial(\rho_{fs}q_{pr})}{\partial r}+\frac{\rho_{fs}q_{pr}}{r}+\frac{\partial(\rho_{fs}q_{pz})}{\partial z}\right)rdrd\theta dz \quad (7)$$
$$-\left(\frac{\partial}{\partial z}(\varphi D\frac{\partial\rho_{fs}}{\partial z})+\frac{\partial}{\partial r}(\varphi D\frac{\partial\rho_{fs}}{\partial r})+\frac{\varphi D}{r}\frac{\partial\rho_{fs}}{\partial r}\right)rdrd\theta dz$$

We assume that the solid particles cannot be compressed, and that the volume of the REV is constant, thus we may deduce the following expression using Formula (2), in such a manner:

$$\frac{\partial(C\varphi)}{\partial t}+\frac{\partial}{\partial r}(Cq_{pr}-\varphi D\frac{\partial C}{\partial r})+\frac{1}{r}(Cq_{pr}-\varphi D\frac{\partial C}{\partial r})+\frac{\partial}{\partial z}(Cq_{pz}-\varphi D\frac{\partial C}{\partial z})=\frac{\dot{m}}{\rho_s} \quad (8)$$

The relationship between porosity change rate and mass-generation term is as follows:

$$\frac{\partial\varphi}{\partial t}=\frac{\dot{m}}{\rho_s} \quad (9)$$

Combining Formulas (8) and (9), we obtain the following:

$$\frac{\partial(C\varphi)}{\partial t}+\nabla\cdot(C\vec{q}_p-\varphi D\nabla C)=\frac{\partial\varphi}{\partial t} \quad (10)$$

For fluidized solid particles, due to the fact that the diffusion effect is comparatively smaller than the advection effect, we may neglect the diffusion effect, thus Formula (10) becomes the following:

$$\frac{\partial(C\varphi)}{\partial t}+\nabla\cdot(C\vec{q}_p)=\frac{\partial\varphi}{\partial t} \quad (11)$$

Formula (11) is the particle balance equation.

We may also deduce the balance equation for the fluid:

$$\frac{\partial[\varphi(1-C)]}{\partial t}+\nabla\cdot[(1-C)\vec{q}]=0 \tag{12}$$

where $\vec{q}$ is the Darcy velocity (m/s).

2.3 Porosity evolution equation

For the sake of simplicity, here we will study the governing equations and present the results using the monomial erosion model:

$$\frac{\partial\varphi}{\partial t}=\lambda\rho_s(1-\varphi)C\parallel q\parallel \tag{13}$$

where λ is a constant, ρ_s is the solid particle density, and $\parallel q\parallel$ is the velocity the mixture, which may be considered as equal to the fluid velocity under a small concentration of fluidized solid particles. The expression shows that the change rate of porosity caused by erosion is proportional to the concentration of fluidized solid particles and the seepage velocity of the mixture.

2.4 Fluid movement equation

Darcy's law for fluid movement in porous medium can be expressed as follows:

$$\vec{q}=-\frac{k}{\eta}(\nabla p+\rho g\nabla z) \tag{14}$$

In this equation, k is the permeability of the porous medium (m^2); $\eta$is the fluid's dynamic viscosity ($Pa\cdot s$); p is the fluid's pressure (Pa), and $\rho$is its density (kg/m^3); and ∇z is a unit vector in the direction over which g acts.

2.5 Particle movement equation

Due to the fact that fluidized solid particles migrate upwardly, their velocity will not be equal to the fluid, because their density is larger than the fluid's. The velocity of the fluidized solid particles under upward transport may be expressed as the difference between fluid velocity and the free settlement velocity of fluidized solid particles in static water. Therefore, we may obtain the following formula:

$$\left.\begin{array}{l} q_{px}=\frac{k(\varphi)}{\eta}\frac{\partial p}{\partial x} \quad q_{py}=\frac{k(\varphi)}{\eta}\frac{\partial p}{\partial y} \\ q_{pz}=\frac{k(\varphi)}{\eta}(\frac{\partial p}{\partial z}+\rho g)-\varphi\sqrt{\frac{4}{3}\frac{d_p(\rho_p-\rho)g}{C_D\rho}} \end{array}\right\} \tag{15}$$

where $u_t = \sqrt{\frac{4}{3}\frac{d_p(\rho_p-\rho)g}{C_D\rho}}$ denotes the free settlement velocity of fluidized solid particles in static water, d_p is the diameter of the particles, and C_D is the dimensionless drag coefficient, which is related to the Reynolds number (Re_p), and $Re_p = \frac{d_p q_p \rho}{\mu}$. JM Ferreira (Ferreira and Chhabra, 1998) introduced a drag coefficient which is suitable within a wide range of Reynolds numbers:$C_D = \frac{24}{Re_p} + 0.5$ $(0 < Re_p < 1 \times 10^5)$.

2.6 Momentum conservation for solid media

We denote that the stress of the solid media is $\overset{\leftrightarrow}{\Sigma}$, displacement is $\vec{u}_s$, body force is $\vec{F}$, and porosity pressure is$p$; then, the momentum conservation equation for solid media may be expressed as follows:

$$-m_s\ddot{\vec{u}}_s + \vec{\nabla}\cdot[\overset{\leftrightarrow}{\Sigma} - \varphi p\overset{\leftrightarrow}{E}] + \vec{F} = \vec{0} \tag{16}$$

where $\overset{\leftrightarrow}{E} = \delta_{ij}\vec{e}_i\vec{e}_j$is a unit tensor, $\delta_{ij}$is Kronecker-δ sign, and $\vec{e}_i(i = 1,2,3)$ is the unit vector along the coordinate axis.

2.7 Auxiliary equations

The relationship between seepage velocity for fluid transport in a porous medium and porosity may be expressed as follows:

$$k(\varphi) = k_0(\frac{\varphi}{\varphi_0})^3(\frac{1-\varphi_0}{1-\varphi})^2 \tag{17}$$

where φ_0 and k_0 are the initial porosity and permeability, respectively.

The relationship between dynamic viscosity of fluid η_0 and dynamic viscosity η of fluid with particles may be expressed by the Einstein formula:

$$\eta(C) = \eta_0(1+2.5C) \tag{18}$$

In summary, we have seven equations, i.e. Formulas (11)∼(18), and seven unknown parameters, i.e. φ, k, p, η, C, $\vec{q}$, $\vec{q}_p$, $\vec{u}_s$, therefore the equations may be closed. Figure 3 shows the coupling relationship between the model equations, thus we may see that this model includes seepage and erosion, which together form the fluid-solid coupling mechanical model for karst collapse columns.

3 Numerical simulation model

3.1 Numerical simulation scheme

Based on the mechanical model discussed above, we can import it into the coupled software program COMSOL Multiphysics, to study the water outburst problem for

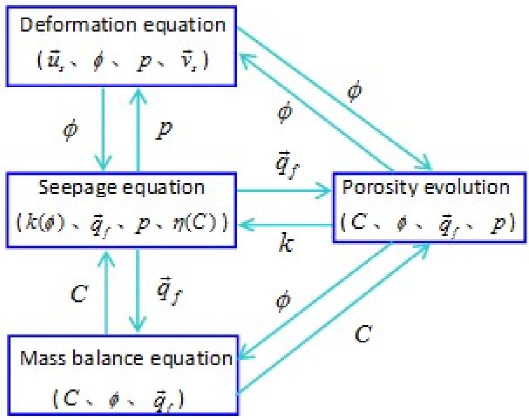

Figure 3: Coupling relationships between model equations

karst collapse columns.

The numerical model is shown in Figure 4. The length, width and height of the model are 250, 100 and 115 m, respectively, the diameter of the karst collapse column is 20 m, and the height is 40 m. There is a confined aquifer in the bottom and the water pressure is 4 MPa. At the top is the coal seam. The water pressure for the mined-out area will be 0 MPa. The left and right sides of the model are the impermeable boundaries. The initial particle density is $C_0 = 0.01$. The other parameters of the model are shown in Table 1.

Furthermore, we consider karst collapse columns as heterogeneous materials, and the distribution of rock porosity may be described by means of Weibull distribution formula(Tang et al., 2002; Zhu et al., 2004; Yang et al., 2004). The probability density equation in Weibull distribution may be expressed as follows:

$$f(\varphi) = \frac{m}{\varphi_0}\left(\frac{\varphi}{\varphi_0}\right)^{m-1} \exp\left[-\left(\frac{\varphi}{\varphi_0}\right)^{m}\right] \tag{19}$$

where φ indicates the porosity, $\varphi_0$denotes the average porosity, and $m$is the uniformity index. The larger $m$represents a higher level of uniformity. The porosity distribution obtained by the numerical generation method is shown in Figure 4.

3.2 Numerical simulation scheme

In order to study the effects of initial porosity on karst collapse column water outburst, the initial porosity $\bar{\varphi}_0$ of the karst collapse column is set as 0.15, 0.2, 0.25 and 0.3, with the respective model numbers of 1, 2, 3 and 4 (Table 2).

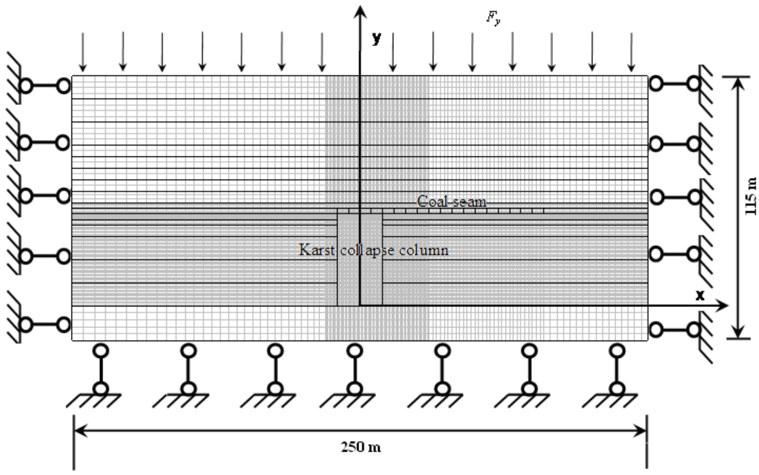

Figure 4: Simulation model for karst collapse column seepage characteristics

4 Numerical simulation results and analysis

4.1 Porosity change characteristics for karst collapse column

Figures 5-8 illustrate the porosity distribution of the karst collapse column and surrounding rock under different initial porosities, while Table 3 and Figure 9 display the average porosity evolution as the distance between the karst collapse columns and working face *d* under different initial porosities.

We may see that the porosity of the karst collapse column gradually evolves and forms main seepage channels with the advancement of the working face. For models with average porosities of $\bar{\varphi}_0 = 0.25$ and $\bar{\varphi}_0 = 0.3$, the distribution rule for seepage channels is as follows: several seepage channels distribute uniformly and display network structures at the bottom of the model, and gradually converge to a main seepage channel at the middle and top of the model. For models with relatively smaller average porosities, the seepage channel evolution is quite slow. For example, no main seepage channel appears in models under$\bar{\varphi}_0 = 0.15$, until the working face advances to 5 m.

We may see from Table 3 and Figure 9 that the porosity changes faster with a larger initial average porosity. When the distance between the working face and Karst collapse column decreases from 20 to 5 m, the initial average porosity for the $\bar{\varphi}_0 = 0.3$ model increases from 0.3038 to 0.4359, with an increase rate of 43.48%; the average porosity for the $\bar{\varphi}_0 = 0.25$ model increases from 0.2543 to 0.3421, with a growth rate of 34.53%; and the growth rates of the $\bar{\varphi}_0 = 0.2$ and $\bar{\varphi}_0 = 0.15$ models

Table 1: Values of the main parameters

Parameter	Value
Water dynamic viscosityη_0	1e-3 (Pas)
Water densityρ	1000 (kg/m^3)
Initial permeabilityk_0	5e-12 (m^2)
Average porosityφ_0	0.15
Particle diameterd_p	1e-5 (m)
Particle densityρ_s	2000 (kg/m^3)
Initial concentrationC_0	0.01
Initial pressurep_0	2 (MPa)
Erosion coefficientλ	1e-3 (m^{-1})
The maximum porosity$\varphi_{\max}$	0.3
Weibull uniformity index m	5

Table 2: Parameters for the schemes in the numerical simulation

Model number	1	2	3	4
$\bar{\varphi}_0$	0.15	0.2	0.25	0.3

are only 12.69 and 6.99%, respectively. In fact, a larger initial average porosity signifies larger permeability and morefluidized solid particles, which results in a more rapid change in porosity.

Table 3: Average porosity $\bar{\varphi}$ change rule for karst collapse columns with d and $\bar{\varphi}_0$

d/m	$\bar{\varphi}_0$			
	0.15	0.2	0.25	0.3
20	0.1517	0.2017	0.2543	0.3038
15	0.1540	0.2052	0.2620	0.3167
10	0.1574	0.2124	0.2888	0.3559
5	0.1623	0.2273	0.3421	0.4359

4.2 Water inflow change characteristics

Figures 10-13 illustrate how the seepage velocity and vectors change with the advancement of the working face, and Table 4 and Figure 14 display how water in-

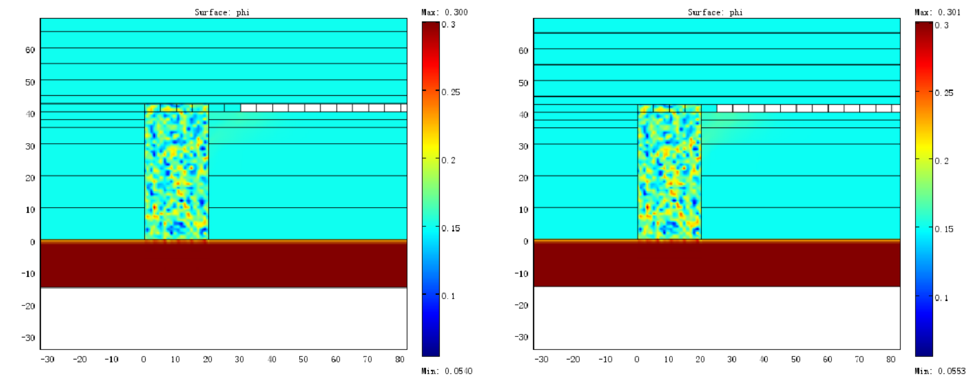

(a) $d = 10$m (b) $d = 5$m

Figure 5: Porosity distribution for karst collapse column and surrounding rock ($\bar{\varphi}_0 = 0.15$)

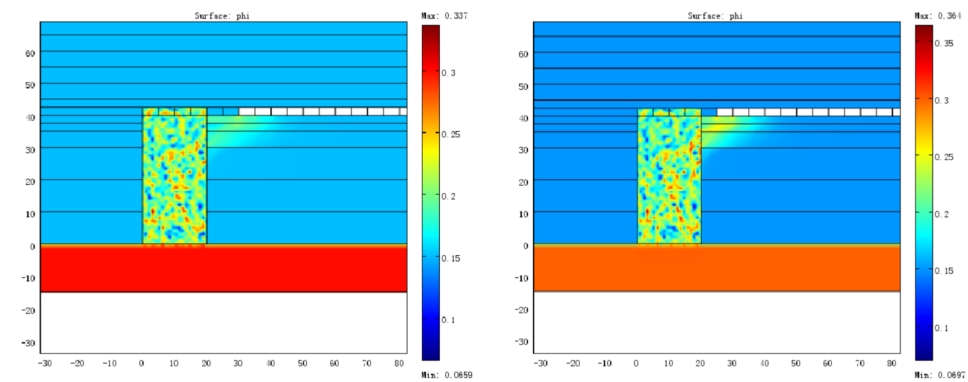

(a) $d = 10$m (b) $d = 5$m

Figure 6: Porosity distribution for karst collapse column and surrounding rock ($\bar{\varphi}_0 = 0.2$)

flow Q changes with the distance between the karst collapse column and working face d. As may be seen, model seepage velocity increases with the growth in the initial average porosity for the karst collapse column. When the working face advances to 10 m away from the karst collapse column, the seepage velocities for the $\bar{\varphi}_0 = 0.15$and $\bar{\varphi}_0 = 0.2$ models are only $4.159 \times 10^{-4}$and 1.768×10^{-3}m/s, respectively, while those for the $\bar{\varphi}_0 = 0.25$ and $\bar{\varphi}_0 = 0.3$ models reach up to 0.0244 and 0.0392 m/s. At the same time, the seepage vectors for the $\bar{\varphi}_0 = 0.15$ and $\bar{\varphi}_0 = 0.2$

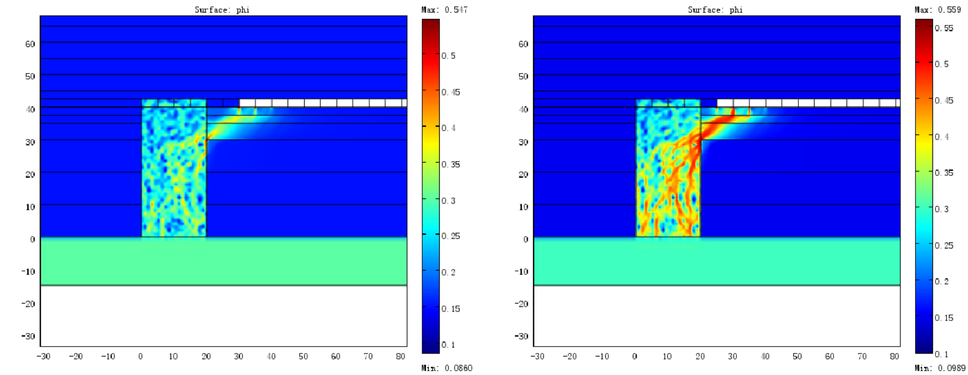

(a) $d = 10$m (b) $d = 5$m

Figure 7: Porosity distribution for karst collapse column and surrounding rock ($\bar{\varphi}_0 = 0.25$)

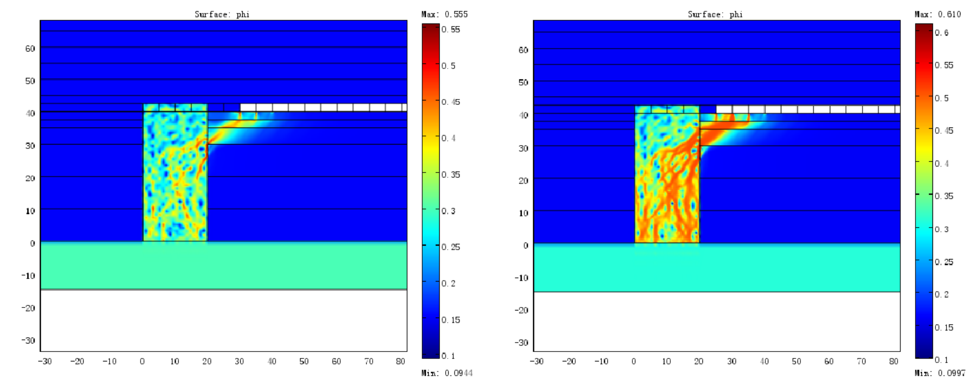

(a) $d = 10$m (b) $d = 5$m

Figure 8: Porosity distribution for karst collapse column and surrounding rock ($\bar{\varphi}_0 = 0.3$)

models distribute uniformly, while those for the $\bar{\varphi}_0 = 0.25$ and $\bar{\varphi}_0 = 0.3$ models behave significantly differently, especially in the top of the karst collapse column, where the seepage vectors are much larger than those in other areas.

We may see from the tables and figures that water inflow increases with the growth of initial average porosity in the karst collapse columns. When the working face advances to 20 m away from the karst collapse column, the water inflow for the $\bar{\varphi}_0 = 0.3$ and $\bar{\varphi}_0 = 0.15$ models are 0.7353 m^3/min and 0.1566 m^3/min, where the

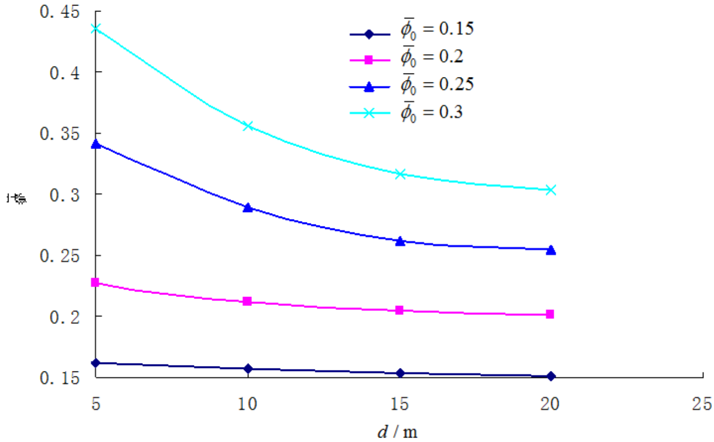

Figure 9: Average porosity $\bar{\varphi}$ for karst collapse column with d and $\bar{\varphi}_0$

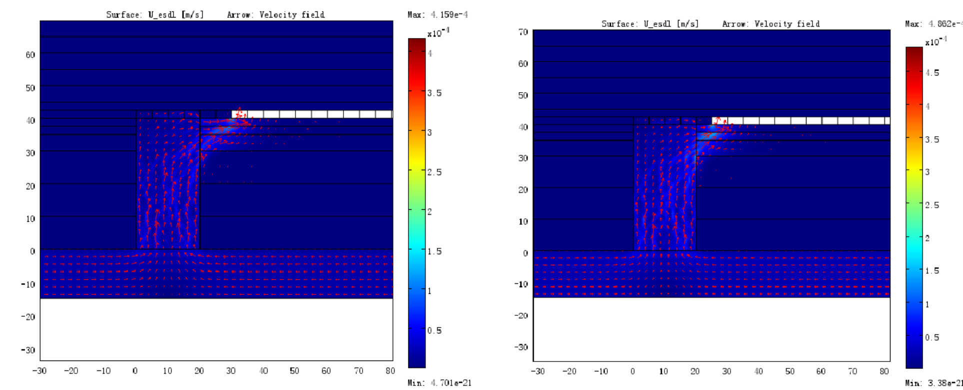

(a) $d = 10$m (b) $d = 5$m

Figure 10: Seepage velocity distribution for collapse column and surrounding rock ($\bar{\varphi}_0 = 0.15$)

former is 4.7 larger than the latter; when the distance decreases to 10 m, these numbers become 8.4587 and 0.3919 m^3/min, respectively, thus causing the gap to reach 21.6. This indicates that water inflow increases more quickly for models with larger initial average porosities, and that water outburst risk increases as the distance between working face and karst collapse column decreases.

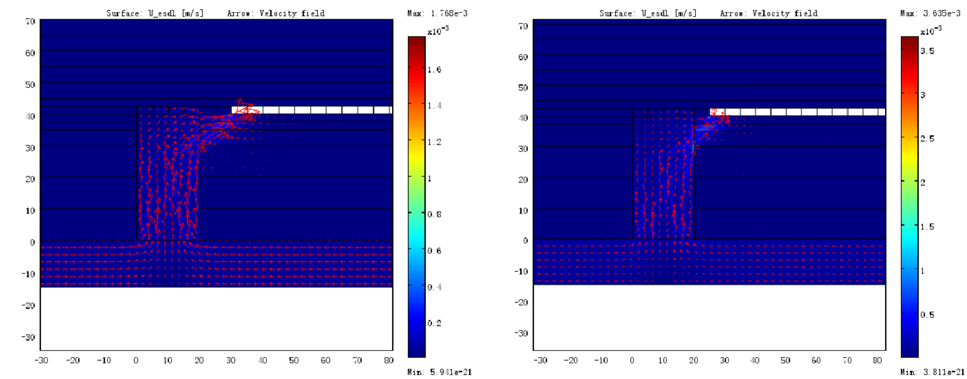

(a) $d = 10$m (b) $d = 5$m

Figure 11: Seepage velocity distribution for collapse column and surrounding rock ($\bar{\varphi}_0 = 0.20$)

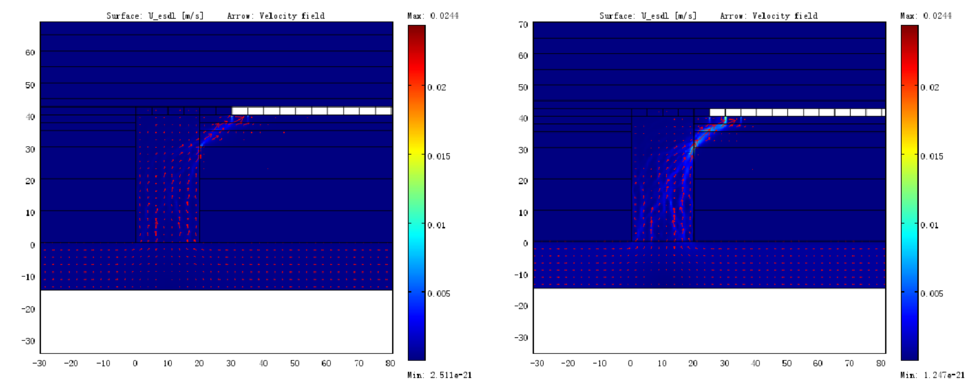

(a) $d = 10$m (b) $d = 5$m

Figure 12: Seepage velocity distribution for collapse column and surrounding rock ($\bar{\varphi}_0 = 0.25$)

Table 4: Water inflow change rules for d and $\bar{\varphi}_0$

d/m	$\bar{\varphi}_0$			
	0.15	0.2	0.25	0.3
20	0.1566	0.2101	0.4639	0.7353
15	0.2580	0.4154	1.2095	2.1558
10	0.3919	0.8350	3.8065	8.4587
5	0.5609	1.7726	12.0554	25.2504

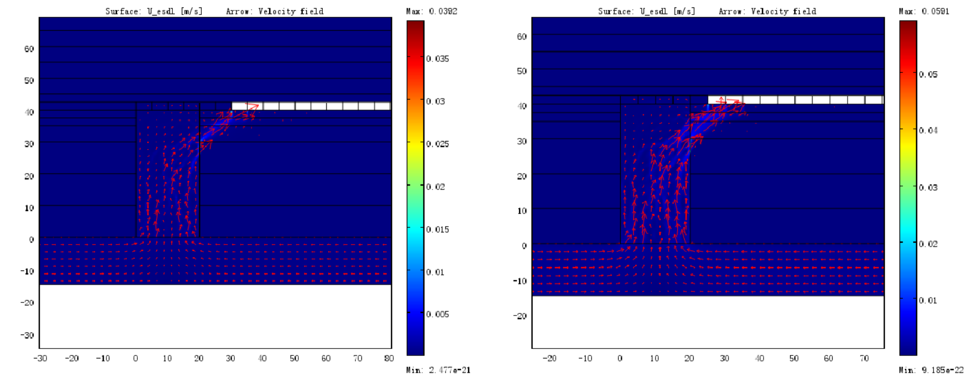

(a) $d = 10$m (b) $d = 5$m

Figure 13: Seepage velocity distribution for collapse column and surrounding rock ($\bar{\varphi}_0 = 0.30$)

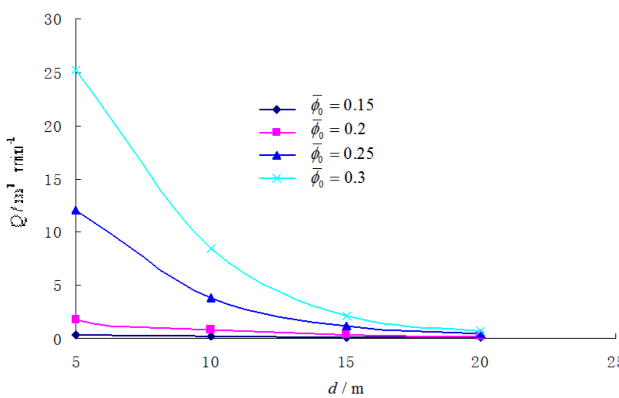

Figure 14: Water inflow change curves for d and $\bar{\varphi}_0$

4.3 Effects of initial average porosity on migration of particles

We may see from Table 5 and Figure 15 that the particle flow rate increases with the growth in initial average porosity for the karst collapse column. When the working face advances to 10 m away from the karst collapse column, the particle flow rate increases sharply from 0.0318 to 0.5453 m^3/min as the porosity grows from 0.15 to 0.3; this indicates that the larger the initial average porosity is, the higher the particle flow rate will be.

On the other hand, particle flow rate Q_p increases as the distance between karst collapse column and working face decreases. Taking the $\bar{\varphi}_0 = 0.2$ model as an example, when the working face advances from 20 to 5 m away from the karst collapse column, the particle flow rate increases sharply from 0.0159 to 0.1381 m^3/min, with the latter 8.7 times larger than the former. The model shows that the water outburst risk grows as the distance between the working face and karst collapse column decreases.

We may see from Table 5 and Figure 15 that the particle flow rate increases with the growth in initial average porosity for the karst collapse column. When the working face advances to 10 m away from the karst collapse column, the particle flow rate increases sharply from 0.0318 to 0.5453 m^3/min as the porosity grows from 0.15 to 0.3; this indicates that the larger the initial average porosity is, the higher the particle flow rate will be.

On the other hand, particle flow rate Q_p increases as the distance between karst collapse column and working face decreases. Taking the $\bar{\varphi}_0 = 0.2$ model as an example, when the working face advances from 20 to 5 m away from the karst collapse column, the particle flow rate increases sharply from 0.0159 to 0.1381 m^3/min, with the latter 8.7 times larger than the former. The model shows that the water outburst risk grows as the distance between the working face and karst collapse column decreases.

Table 5: Particle migration velocity Q_p change for d and $\bar{\varphi}_0$

d/m	$\bar{\varphi}_0$			
	0.15	0.2	0.25	0.3
20	0.0153	0.0159	0.0402	0.0533
15	0.0215	0.0322	0.1175	0.1790
10	0.0318	0.0672	0.2942	0.5453
5	0.0450	0.1381	0.5869	1.1118

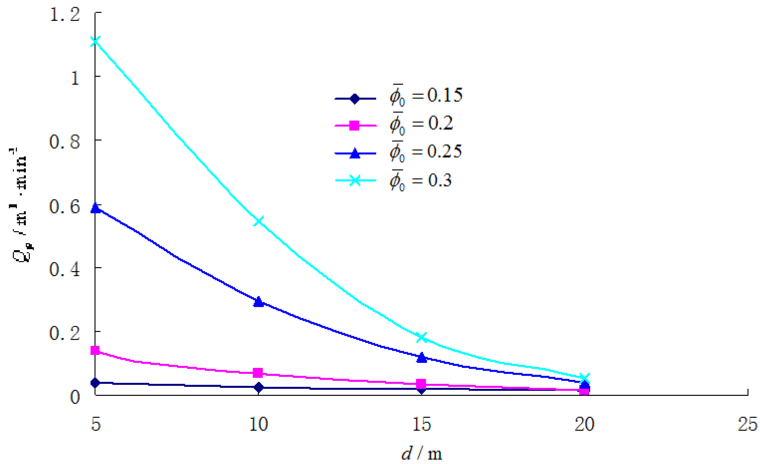

Figure 15: Particle migration velocity Q_p change curves for d and

4.4 Plastic area change rule

We may see from the figures that the plastic area increases as the working face advances, especially in the karst collapse column; when the working face advances to 20 m away from the karst collapse column, only a small area rock failed, whereas when the distance decreased to 5 m, a much larger area in the karst collapse column was destroyed. This indicates that the water outburst risk increases as the working face advances to the karst collapse column.

5 Conclusions

This paper mainly studied the seepage property of karst collapse columns and water outburst mechanism induced by porosity development, by means of building a particle erosion model. The main conclusions may be summarized as follows:

(1) Particles in the karst collapse column will erode and migrate under the effect of fluid as the time, the porosity, water inflow and particle migration velocity grow, and eventually a main seepage channel will form.

(2) The seepage capacity for karst collapse columns initially grows slowly, then the water inflow increases quickly with the erosion and migration of the particles. In order to prevent this from occurring, measures must be taken to reduce the erosion of particles in karst collapse columns, such as grouting.

(3) The effects of initial average porosity on porosity evolution water inflow and

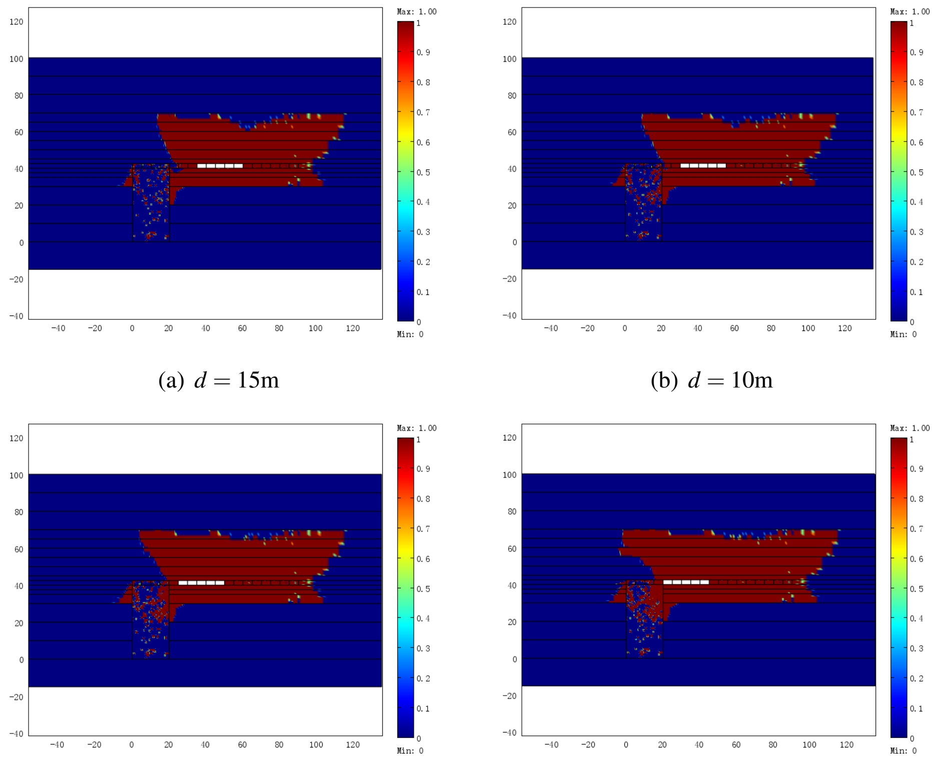

(a) $d = 15$m (b) $d = 10$m

(c) $d = 5$m (d) $d = 0$m

Figure 16: Plastic area change with the advancement of the working face

particle migration velocity are quite large. Larger initial average porosity will induce a higher porosity evolution ratio as well as larger water inflow and particle migration velocity.

(4) Plastic areas increase in size as the working face advances, especially in karst collapse columns. As the working face advances, a larger area of the Karst collapse column is destroyed, which indicates that the water outburst risk increases as the working face advances to the karst collapse column.

The theoretical analysis and simulation results in this paper may provide significant reference for the study of karst collapse column seepage properties and water outburst control.

Acknowledgements

This project is supported by the National Basic Research Program of China (Nos. 2013CB227900 and 2012CB723100), and the National Natural Science Foundation of China (Nos. U1261201, 51104059 and 51074067).

References

Benmebarek, N.; Benmebarek, S.; Kastner, R. (2005): Numerical studies of seepage failure of sand within a cofferdam. *Computers and Geotechnics*, vol.32, pp.264-273.

Bouchelaghem, F.; Jozja N. (2009): Multi-scale study of permeability evolution of a bentonite clay owing to pollutant transport. *Engineering Geology*. Vol.108, pp.119-132.

Ferreira, J. M.; Chhabra, R. P. (1998): Accelerating motion of a vertically falling sphere in incompressible Newtonian media: an analytical solution. *Powder Technology*, vol.97, pp.6-15.

Habib, M. A.; Badr, H. M.; Ben, R. (2007): Erosion rate correlations of a pipe protruded in an abrupt pipe contraction. *International Journal of Impact Engineering*, vol.34, pp.1350-1369.

Papamichos, E.; Vardoulakis, I. (2005): Sand erosion with a porosity diffusion law. *Computers and Geotechnics*, vol.32, pp.47-58.

Peter, O.; John C.; Enrique, M.; A. Sen (1987): Geochemical self-organizationII: The reactive-infiltration instability. *American Journal of Science*, vol.287, pp.1008-1040.

Tang, C.A; Tham, L.G.; Lee, P.K.K.; Yang, T.H.; Li, L.C. (2002): Coupled analysis of flow, stress and damage (FSD) in rock failure. *International Journal of Rock Mechanics & Mining Sciences*, vol.39, pp.477-489.

Tang, J. H; Bai H. B; Yao, B. H.; Wu, Y. (2011): Theoretical analysis on water outburst mechanism of concealed collapse. *International Journal of Mining Science and Technology*, vol.21, pp.57-60.

Vardoulakis, I.; Stavropoulou, M.; Papanastasiou, P. (2007): Hydro-Mechanical Aspects of the sand production problem. *Transport in porous media*, vol.22, pp.225-244.

Wang, J. C.; Xu, X. B.; Wang, G. M..(2010): Development and Application of Simulation Test System for Water Inrush from the Water-Conducting Collapse Column. *Journal of Mining & Safety Engineering*, vol.27, pp.305-309.

Wang, J.; Wan, R.G. (2004): Computation of sand fluidization phenomena using stabilized finite elements. *Finite Elements in Analysis and Design*. vol.40, pp.1681-1699.

Yang, T. H.; Chen, S. K.; Zhu, W. C.; Meng, Z. P.; Gao, Y. F. (2008): Water inrush mechanism in mines and nonlinear flow model for fractured rocks. *Chinese Journal of Rock Mechanics and Engineering*, vol.27, pp.1411-1416.

Yang, T.H.; Tham, L.G.; Tang, C.A.; Liang, Z.Z.; Tsui, Y. (2004): Influence of heterogeneity of mechanical properties on hydraulic fracturing in permeable rocks. *Rock Mechanics and Rock Engineering*, vol.37, pp.251-275.

Yasuhara, H.; Elsworth, D.. (2006): A numerical model simulating reactive transport and evolution of fracture permeability. *International Journal for Numerical and Analytical Methods in Geomechanics*. Vol.30, pp.1039–1062.

Zhu, W.C.; Tang, C.A. (2004): Micromechanical model for simulating the fracture process of rock. *Rock Mechanics and Rock Engineering*, vol.37, pp.25-56.

Zhu, W. C.; Wei, C. H.; Zhang, F. Z.; Yang, T. H. (2009): Investigation of water outburst from Karst subsidence column by using a coupled hydro-mechanical model. *Chinese journal of underground space and Engineering*, vol.5, pp.928-933.